Composites Part B 233 (2022) 109662

Contents lists available at ScienceDirect

Composites Part B

journal homepage: www.elsevier.com/locate/compositesb

A novel three-dimensional boron phosphide network for thermal management of epoxy composites

Jing He [a,b,c], Hua Wang [a,**], Yi Gong [a], Xingyou Tian [a,***], Zhiliang Zhang [c], Jianying He [c,*]

[a] Key Lab of Photovoltaic and Energy Conservation Materials, Institute of Solid State Physics, HFIPS, Chinese Academy of Sciences, Hefei, 230031, China
[b] University of Science and Technology of China, Hefei, 230026, China
[c] Department of Structural Engineering, Faculty of Engineering, Norwegian University of Science and Technology (NTNU), 7491, Trondheim, Norway

ARTICLE INFO

Keywords:
3D-BP@Ni
ER/3D-BP@Ni composite
Isotropic thermal conductivity
Compatible coefficient of thermal expansion

ABSTRACT

Recently, construction of effective three-dimensional (3D) heat transfer networks inside polymer has emerged as a promising design strategy to improve the isotropic thermal conductivity for electronic packaging materials. Hexagonal boron nitride (BN) sheets are popular carriers for constructing 3D networks. But removing overheat capability of BN was greatly sacrificed due to size limitation when constructing 3D network. Herein, a novel 3D heat-transferring network, interconnected boron phosphide (BP) grains in-situ growing on Ni foam, was designed to alternate 3D BN network. An isotropic 3D-BP@Ni network with high-quality and integrity was successfully fabricated by a simple high temperature treatment. The synthesized 3D-BP@Ni was incorporated into epoxy resin (ER) by infiltration to fabricate composites. ER/3D-BP@Ni composite, with strong interfacial adhesion between epoxy and 3D-BP@Ni, achieved a high thermal conductivity of 2.01 W/(mK), which corresponded to 908.53% and 402.00% enhancement compared to pure epoxy and ER/Ni composite. The coefficient of thermal expansion (CTE) of the composite reached as low as 26.95 $\times$ 10^{-6}/°C, much smaller than epoxy of 60.69 $\times$ 10^{-6}/°C and ER/Ni composite of 59.42 $\times$ 10^{-6}/°C. The designed ER/3D-BP@Ni composite has distinguished heat removal and CTE with semiconductors from traditional polymer composites containing 3D BN network. This strategy is promising to promote the development of electrical packaging materials with high isotropic thermal conductivity.

1. Introduction

With continued advancement of electronic devices, micro-chips would consume hundreds of megawatts of power in computation and convert almost all energy into heat, which was equivalent to the output of a small nuclear plant [1,2]. Increasing heat has been looming as the biggest obstacle to computing technology and restricted the development of electronic industry [3]. To achieve a good heat removal, engineers have explored many new cooling pathways [4–6], and researchers are committed to developing passive heat dissipation packaging material [7]. Polymers as the common electronic packaging materials have been favored for a long time due to their low-cost, light weight, and easy processability [8,9]. But the low intrinsic thermal conductivity of polymer made it difficult to match the heat dissipation capacity required by current micro-chips, resulting in that a large number of works about polymer incorporating fillers with high intrinsic thermal conductivity sprung up [10–13]. Unfortunately, many fillers inside polymer not only failed to achieve the satisfactory heat dissipation performance, but also increased the cost of polymer composites [14]. There are huge demands to develop novel methods for preparing polymer composites with high thermal conductivity.

Filling a lot of thermal conductive materials or constructing effective heat transferring structures, according to the widely accepted theory of thermal conduction pathways, were plausible solutions to improve the thermal conductivity of polymer composites [15,16]. The traditional method of high-loading fillers was usually at the expense of reducing other performance of polymer composites [17]. Therefore, constructing three-dimensional (3D) interconnected networks have received wide attention [18,19]. Effective heat transferring structures provide continuous thermal conduction pathways in polymer due to ordered

* Corresponding author.
** Corresponding author.
*** Corresponding author.
E-mail addresses: wanghua@issp.ac.cn (H. Wang), xytian@issp.ac.cn (X. Tian), jianying.he@ntnu.no (J. He).

https://doi.org/10.1016/j.compositesb.2022.109662
Received 12 September 2021; Received in revised form 14 January 2022; Accepted 17 January 2022
Available online 21 January 2022

physical or chemical features [20]. Carbon materials (graphene [21], carbon nanotube [22], and carbon fiber [23]) with unique flexibility and ultrahigh anisotropic thermal conductivity have been common 3D networks carries. Specially, graphene with the conjugated molecular plane structure can provide an ideal two-dimensional (2D) pathway for phonon transport [16]. Many complicated methods, such as ice-templated [24], self-assembly [25], and chemical vapor deposition [26], were used to construct 3D graphene network. But the weak interaction between graphene layers might damage the isotropic thermal conductivity of 3D graphene network. The high electrical conductivity of graphene is also a drawback as the electrical packaging material. In addition to carbon materials, it is common to use ceramics with high thermal conductivity to form 3D network to improve the thermal conductivity of polymer [27]. Among others, hexagonal boron nitride (BN) is most popular due to the similar structure to graphene [19,28]. Even though the modification of BN is very hard, some works using BN as thermal conductor have achieved satisfied results [29–31]. Generally, large-size BN sheets make it easy to achieve a substantial increase in thermal conductivity of polymer composites than small-size BN sheets [32]. However, it is very difficult to construct a 3D large-size BN sheets network because their geometric characters could lead to stack easily [33].

Thence, exploring new materials easy to construct high isotropic thermal conductivity 3D network is hot. Boron phosphide (BP) as a common cubic III–V compound is one of candidate materials. It is made up of two lightweight and abundant elements of boron and phosphorus that exhibits strong covalent bonding. Ordinarily, nonmetallic materials with strong covalent bond endow high isotropic thermal conductivity in the light of the Slack's classic guidelines [34,35]. But since BP was first synthesized in 1957, early researches on thermal conductivity of BP are sparse [36]. Heat transfer of BP has not been paid attention until the high thermal conductivity of BP single crystals was verified [37–39]. Theoretically, BP single crystals were predicted to have an excellent thermal conductivity 580 W/(mK) at room temperature from the first-principles calculation [40]. Experimentally, the thermal conductivity of 350 W/(mK) in BP natural crystal was measured at room temperature by Slack [34]. Later, the measured value was updated to ~400 W/(mK) by Kumashiro et al. [41]. The advancement in the thermal characterization technique led to higher thermal conductivity reported. Hu's group obtained 460 W/(mK) with time-domain thermoreflectance (TDTR) [37]. Zheng et al. got a new record-high 490 W/(mK) at room temperature [38]. Different from 2D graphene and BN, BP has not only high isotropic thermal conductivity, but also exceptional chemical refractory properties, high thermal stability, and large elastic modulus as well as a unique potential to be used in nuclear and radiation detectors [42–44]. The coefficient of thermal expansion (CTE) of BP ($3.2 \pm 0.2 \times 10^{-6}/^{\circ}C$) is compatible with many commercial semiconductors, such as Si, SiC, GaN, and GAs, in comparison in diamond [45]. Thus, BP is considered as a good candidate and promising material in high power microelectronics devices for harsh environments.

Here, combining with 3D networks, a novel 3D-BP@Ni network was constructed to achieve high isotropic thermal conductivity and suitable CTE value of polymer composites. Commercial Ni foam was used as a 3D framework to support the growth of BP grains. Synthetic continuous and high-quality 3D-BP@Ni can avoid the limitation of Ni foam, such as low thermal conductivity and inappropriate CTE value. What is more attractive is that 3D-BP@Ni not only has free size but also has a popular one-step fabrication process, outperforming 3D BN networks. Epoxy resin, a currently commercial integrated circuit substrate material, was selected as the polymer matrix. As for the preparation of the composites, infiltration was a good choice since it is damage free to the network. The obtained composites were endowed with high thermal conductivity and an appropriate CTE. In summary, our work here shows the one-step synthesized 3D-BP@Ni network achieved excellent properties in epoxy, indicating its wide application in thermal management.

2. Raw materials and methods

2.1. Synthesis of 3D-BP@Ni

Ni foam (Supplementary, S1, Figs. S1(a) and (b)) purchased from New Energy Materials Co., Ltd. was cleaned by dilute hydrochloric acid (0.5 wt%) to remove the oxide layer. It was washed in the ethanol for 10 min and dried in vacuum. B powders were provided by Macklin Biochemical Co., Ltd. and ultrasonically dispersed in ethanol at a concentration of 10 mg/ml. The pretreated Ni foam was immersed in the B/ethanol solution for 5 min, and then dried in vacuum. B powders were loaded on the Ni foam to form the B/Ni foam (Supplementary, S1, Figs. S1(c) and (d)). The volume fraction of B powders is 10.94 vol%. Red phosphorus (99.999%, metal basic, Aladdin) and the B/Ni foam were immediately flame-sealed in a quartz tube under 1.0×10^{-3} Pa. The sealed quartz tube was horizontally placed in a tube furnace (MTI KJ GSL−1400X, Hefei, China) with heated up to 1100 °C for 18h, and slowly cooled to room temperature. At last, a large area 3D-BP@Ni interconnected network (15mm × 60 mm) was obtained, as shown in Fig. 1(a).

2.2. Preparation of ER/3D-BP@Ni composite

The ER/3D-BP@Ni composite was fabricated by an infiltration method. Proportional epoxy (E51, purchased from Aladdin) and curing agent (Methyltetrahydrophthalic anhydride, provided by Macklin) were poured into a beaker and stirred magnetically at 40 °C for 30 min. The obtained 3D-BP@Ni foam was put into a silicone mold, and then the mixed ER was also poured into the mold. The whole mold was placed in a vacuum oven at 40 °C overnight to remove air in the system and also made 3D-BP@Ni fully infiltrated by epoxy. Subsequently, they were cured at in stages 120 °C for 2h, 150 °C for 2h, and 180 °C for 2h, sequentially. The obtained composites were polished into regular spare electronic substrate materials by a polishing machine. The untreated Ni foam was also prepared into ER/Ni composites according to the above steps for comparison. The schematic illustration of the whole preparing process was shown in Fig. 1(a).

2.3. Characterization

The fabricated ER/3D-BP@Ni composite was cryosectioned to analyze the microstructure and the element distribution by a transmission electron microscope (TEM, JEM-2100). The micromorphologies of 3D-BP@Ni foam and the obtained composites were characterized by a scanning electron microscopy (SEM, Sirion-200). Raman spectrum of 3D-BP@Ni foam was recorded using a confocal Raman microscope employing a laser with a wavelength of 633 nm and excitation power of 1%. X-ray diffraction pattern of the samples was taken on the x-ray diffractometer (XRD, Rigaku Smartlab 9 kW). The scanning was performed from 5° to 80° at room temperature.

The thermal conductivity of the composites was measured on steady state thermal conductivity meter (Hot Disk, TPS 2200). The samples with the same size of 15mm × 15mm × 1 mm have been polished for better contrast with the probe of Hot Disk. To guarantee the credibility of the measured results, each thermal conductivity was measured three times and the average values were calculated and adopted. The real-time temperature of the composites was monitored by an infrared thermal imaging camera (ITI, CEM DT-980) and the thermal images were captured. The composites were placed on a variable-voltage constant temperature resistor (12 V, 6-8 W, ~60 °C) to simulate the electronic device and record the temperature rising and distribution of the composites surface.

The dimensional stability of the composites was evaluated by the CTE values. The CTE value of the composites was obtained by a thermomechanical analysis (TMA, Q400 TA) in nitrogen atmosphere with a flow rate of 20 mL/min. The thermal stability of the composites was

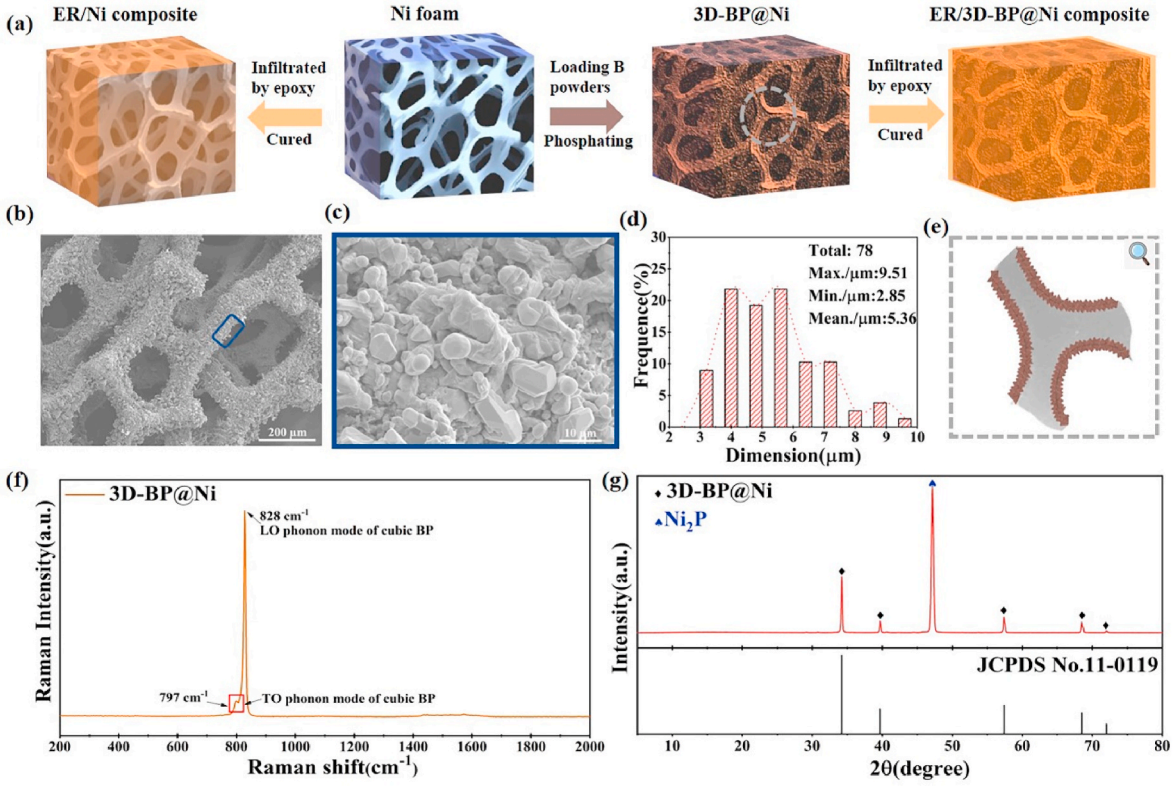

Fig. 1. (a) Schematic illustration of the procedure to prepare 3D-BP@Ni foam and ER composites, (b) the low magnification SEM image of 3D-BP@Ni foam, (c) the high magnification SEM image of 3D-BP@Ni foam, (d) the size distribution of BP grains, (e) the schematic illustration of 3D-BP@Ni foam, (f) Raman spectrum of 3D-BP@Ni foam, (g) XRD pattern of 3D-BP@Ni foam.

measured on thermo-gravimetric analyses (TGA, Q5000 IR). The heat rate was 10 °C/min under the nitrogen atmosphere. The mechanical property of ER composites was tested by the GMT-4204 testing machine at a speed of 2 mm/min.

3. Results and discussion

3.1. 3D-BP@Ni

Ni powders are the common flux for crystal synthesis, including BP [37,43]. After B powder loading and phosphating process at high temperature, 3D-BP@Ni duplicated the interconnected structure of Ni foam, as schematically shown in Fig. 1(a). The macro-morphology of 3D-BP@Ni (low magnification SEM image, Fig. 1(b)) revealed the continuity and the integrity of the structure. The BP crystals grew tightly along the whole foam, as shown in SEM images with different magnifications of Fig. S2. In the high magnification SEM image (Fig. 1(c)), BP grains of a few microns in size were in close contact with each other. The size of 78 BP grains in Fig. 1(c) is calculated by nano measurer 1.25 and the size distribution of BP grains was illustrated in Fig. 1(d), which indicates the mean size of BP grains is 5.36 μm. SEM images were also confirmed that the Ni foam substrate was completely covered by BP grains. The element mapping of the cross-section of 3D-BP@Ni network showed that the Ni element was surrounded by P element in Fig. S3. For the improvement of phonon transferring speed, not only a continuous network is required, but also the high-quality crystal. The microscopic illustration of 3D-BP broadening Ni skeleton was shown in Fig. 1(e). The Raman spectrum of 3D-BP@Ni shown in Fig. 1(f) only exhibited two peaks: a strong LO (longitudinal optical) phonon mode at 828 cm^{-1} and a weak TO (transverse optical) phonon mode at 797 cm^{-1} of cubic BP crystals [46]. No additional peaks were observed. The Raman full-width at half-maximum (FWHM) of 3D-BP@Ni LO mode was obtained by non-linear fitting. The FWHM value of 3D-BP@Ni reached 9.37 cm, lower than FWHM values (>10 cm) of BP crystals synthesized at higher temperature [47,48]. The narrow peak width also revealed the good crystalline quality of BP. In addition, the powder XRD pattern of 3D-BP@Ni (Fig. 1(g)) showed five characteristic diffraction peaks at 34.2°, 39.7°, 57.4°, 68.5°, and 72°, corresponding to (111), (200), (220), (311), and (222) planes of cubic BP crystal (JCPDS No. 11-0119) [49]. The sharp and narrow XRD peaks of 3D-BP@Ni further confirmed the high quality of the synthesized BP particles. It was noted that a strong characteristic diffraction peak at 47.2° corresponded to Ni_2P. According to the growth mechanism of BP crystal synthesized by metal flux method, the presence of Ni_2P is necessary [50]. In this work, Ni_2P as a part of the substrate framework was inside 3D-BP@Ni. Since the thickness of BP layer grown on the pretreat Ni foam was only a few microns (Supplementary, S1, Fig. S4), Ni_2P can be easily characterized in XRD pattern.

3.2. ER/3D-BP@Ni composite

Ni foam and 3D-BP@Ni were infiltrated in epoxy to cure into ER/Ni and ER/3D-BP@Ni composites, as shown in Fig. 1(a). XRD pattern of ER/Ni composite showed the sharp characterized peaks belonging to Ni foam (JCPDS No. 65-2865) and a broad characterized peak presenting epoxy in Fig. S5(a). Similarly, XRD pattern of ER/3D-BP@Ni composite showed the characterized peaks belong to BP, Ni_2P, and epoxy in Fig. S5 (b). The cross-section morphologies of ER/Ni and ER/3D-BP@Ni composites were investigated by SEM in Fig. 2. The fissures at the interface junction were clearly visible between Ni foam and epoxy in Fig. 2(b) and (c). Compared to ER/Ni composite, ER/3D-BP@Ni composite has better interfacial adhesion between 3D-BP@Ni and epoxy in Fig. 2(d), (e) and (f). The surface of 3D-BP@Ni is rough according to Fig. 1 (b) and (c) and Fig. S2. When the epoxy is applied to the rough surface of 3D-BP@Ni, it

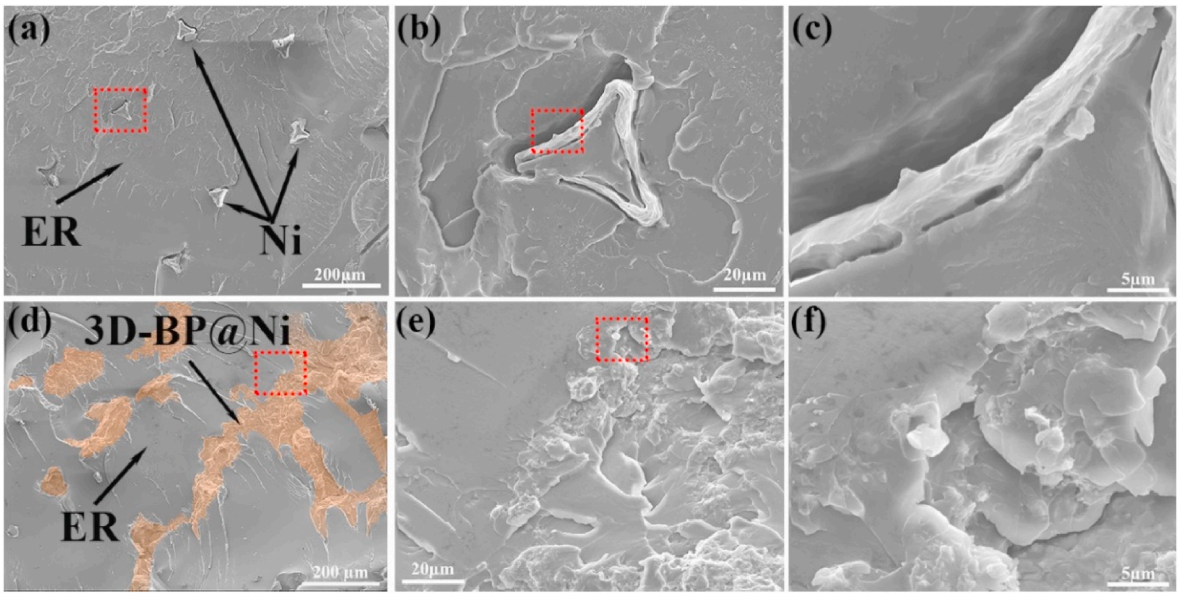

Fig. 2. The cross-sectional SEM images of ER composites: (a), (b), and (c), ER/Ni composite; (d), (e), and (f), ER/3D-BP@Ni composite.

conforms to the rough surface and tends to fill up the unevenness of the surface [51]. Consequently, the mechanical interlock was formed between 3D-BP@Ni and epoxy after a cured process. Mechanical interlock endowed the better interfacial adhesion in ER/3D-BP@Ni composite than ER/Ni composite. As shown in Fig. 2 (e) and (f), no voids can be observed in ER/3D-BP@Ni composite. It was obvious that the open pores in 3D-BP@Ni were fully sealed by epoxy. The strong interface and dense structure in ER/3D-BP@Ni composite was conducive to reduce the interfacial thermal resistance and improve the phonon transferring speed.

To further understand the micro-structure and distribution of 3D-BP@Ni, ER/3D-BP@Ni composite was cryosectioned horizontally for TEM characterization. Although the frozen sectioned process might destroy the network of 3D-BP@Ni, continuously distributed BP grains along the edge of the epoxy slice were still shown in the TEM image (Fig. 3(a)). The continuous distribution of BP grains in micro-structure of ER/3D-BP@Ni composite was elucidated by the corresponding element mapping. The layered electronic image of element mapping is

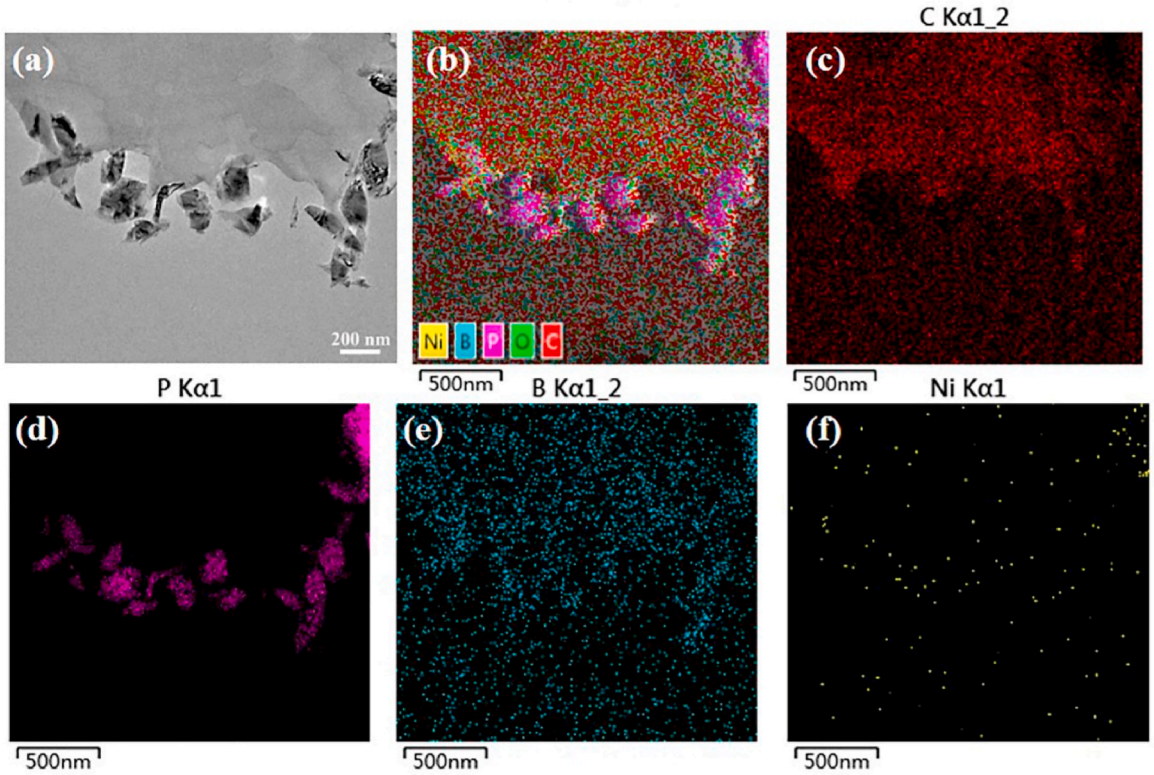

Fig. 3. TEM images and the element mapping of ER/3D-BP@Ni composite: (a) TEM image, (b) EDS layered image, (c) the C element, (d) the P element, (e) the B element, (f) the Ni element.

shown in Fig. 3(b). The C element mapping (Fig. 3(c)) represented the epoxy slice. In Fig. 3(d), the distribution of P element that was also agreement with the BP grains in ER/3D-BP@Ni composite was visible. The corresponding B element (Fig. 3(e)) also appeared along the edge of epoxy slice like the P element. However, the light atomic weight of B resulted in the diluted B element mapping. The Ni element was collected in Fig. 3(f), and little Ni element was shown. The distribution of Ni element was not consistent with P element. Therefore, it was confirmed that 3D-BP@Ni had the better interfacial adhesion with epoxy and BP grains were an excellent cover for Ni foam. The high-magnification SEM image of the ER/3D-BP@Ni composite also showed good interface between epoxy and 3D-BP@Ni (Fig. 2).

3.3. Thermal conductivity of ER composites

A continuous network, especially high thermal conductive structure, in epoxy will significantly improve the thermal conductivity of the composites. The thermal conductivity of the prepared ER/3D-BP@Ni composite was measured at room temperature with the infiltrated epoxy and commercial Ni foam as a reference in Fig. 4. Compared with pure epoxy, ER composites have a prominent enhancement of the thermal conductivity. The incorporation of commercial Ni foam alone increased the thermal conductivity from 0.22 W/(mK) of pure epoxy resin to 0.50 W/(mK) with an improvement of 229.54%. The enhancement of heat dissipation ability in ER/Ni composite indicated that 3D interpenetrating network can construct ordered channels of phonon transmission in disordered epoxy chain. But the intrinsic thermal conductivity of commercial Ni foam could not provide fast pathways for phonon, limiting the speed of phonon transmission. Moreover, the voids between Ni foam and epoxy also caused severe phonon scattering at the interface junction. Severe phonon scattering and poor interfacial compatibility resulted in a high interfacial thermal resistance, limiting the improvement of thermal conductivity. Although commercial Ni foam provided interconnected pathways for phonons in epoxy, the movement of phonons with a slow speed is like a carriage running on the road as shown in Fig. 4(c).

When the BP grains grew into 3D-BP on the pretreated Ni foam by phosphating process as shown in Fig. 4(b), the thermal conductivity of ER/3D-BP@Ni composite was significantly improved to 2.01 W/(mK), 908.53% and 402.00% higher than that of pure epoxy and ER/Ni composite. The breakthrough in the thermal diffusion capability of ER/3D-BP@Ni composite largely benefited from the sound integrity of 3D-BP@Ni and the inherent high thermal conductivity of BP. The continuous 3D-BP@Ni structure contributed high-speed pathways to the phonon transmission in epoxy. Not only that, the sound interface derived from the mechanical interlocking effect will also effectively reduce voids and fissures between epoxy and 3D-BP@Ni. The tight interface and dense structure could significantly decrease the phonon scattering, thereby reducing the interface thermal resistance. In ER/3D-BP@Ni composite, phonon quickly transferred along the continuous and uniform 3D-BP@Ni network like a high-speed train traveling in railways in Fig. 4(c).

It deserved to mention that Ni foam as the template in 3D-BP@Ni network hardly contributed to the thermal conductivity because replacing the template in the 3D network did not affect the thermal conductivity of the prepared composites. In the currently preparing work, Cu foam with the same porosity to Ni foam was used as the template to fabricate 3D-BP@Cu network. The thermal conductivity of ER/Cu composite can reach 6.16 W/(mK), as shown in Fig. S6 in the Supplement. The prepared ER/3D-BP@Cu composite has the thermal conductivity (2.03 W/(mK)) similar to that of ER/3D-BP@Ni composite. The results indicated that the template and derivatives do not impact the thermal conductivity of the composite. The electrical conductivities of the prepared composites (Supplementary, S4) also supported that Ni foam had no contribution. Due to the high electrical conductivity of Ni, ER/Ni composite has a higher electrical conductivity than that of ER and ER/3D-BP@Ni composite. The obtained electrical conductivity of ER/Ni composite is 4.14×10^{-7} S/cm, and that of both ER and ER/3D-BP@Ni composite is less than 2.2×10^{-9} S/cm. Although Ni foam as a part in 3D-BP@Ni can improve the electrical conductivity of ER/3D-BP@Ni composite, it still belongs to the category of insulation ($<10^{-9}$ S/cm). In conclusion, the foam template played a negligible or minor role in the thermal conductivity of the composite. Successful one-step construction of 3D-BP@Ni can effectively improve the phonon velocity and broaden the channels of phonon in epoxy.

The high thermal conductivity of ER/3D-BP@Ni composite confirmed that BP would be an effective alternative to BN, which has been widely applied in electrical materials for removing overheat. In comparison with polymer/3D-BN composites, ER/3D-BP@Ni composite

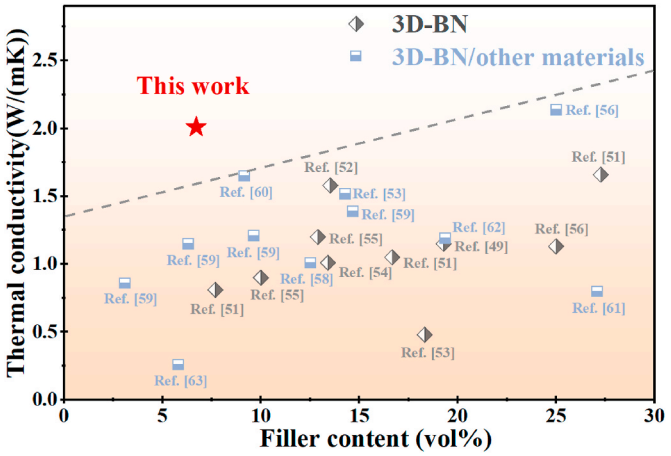

Fig. 5. Comparison of the thermal conductivities of polymer/3D-BN, polymer/3D-BN/other materials and this work as a function of filler volume fraction.

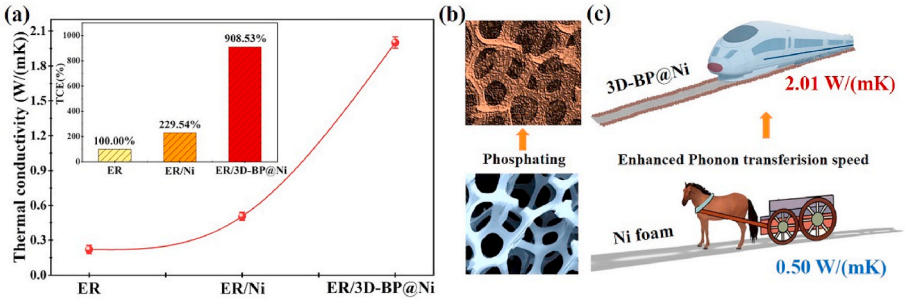

Fig. 4. Thermal conductivity of the composites and schematic illustrations: (a) thermal conductivity, the inset is the thermal conductivity enhancement (TCE), (b) partial schematic illustrations of commercial Ni foam and 3D-BP@Ni, (c) schematic illustrations of phonon transmission in ER/Ni composite and ER/3D-BP@Ni composite.

had the highest thermal conductivity at lowest volume fraction as shown in Fig. 5. Removing-heat capability was greatly sacrificed because the size of 2D hexagonal BN was limited when constructing isotropic 3D network in polymer. Even though other high thermal conductivity materials cooperated with BN to build effective phonon pathways, the enhancement in thermal conductivity of composites has not satisfied the requirement. In Fig. 5, the thermal conductivity of this work was also impressive. It was foreseeable that increasing the volume fraction of BP would drive a fast enhancement in the thermal conductivity of composites. In addition, Table 1 showed BP was superior to BN in constructing a 3D network in polymer composites both in terms of the fabricating process and isotropic thermal conductivity. Complex fabricating processes made them difficult to promote the development of electronic heat-dissipating materials. As a result, 3D-BP was promising to apply in the electrical packaging field due to its simple fabrication and high isotropic thermal conductivity.

3.4. Thermal management capability of ER composites

In addition to thermal conductivity, the actual thermal management capabilities of the composites, as heat dissipation materials on a constant temperature resistance, were characterized by infrared thermal imaging method. The temperature variation as a function of elapsed time was presented in Fig. 6(a). ER/3D-BP@Ni composite represented by the blue curve showed the fastest heating rate and the highest final equilibrium temperature. Moreover, the surface of ER/3D-BP@Ni composite always had the highest temperature at the same elapsed time, confirming that ER/3D-BP@Ni composite possessed the best heat dissipating ability. For epoxy and the composites, the rates at the fastest temperature rising and the specific elapsed time obtained by differentiation were closely related to thermal conductivity, as shown in Table 2.

Table 1
Comparison of thermal conductivity and electrical property for our ER/3D-BP@Ni composite with the reported polymer composites.

Materials	Volume fraction	TC W/(mK)	TCE %	Method, Steps	Year
ER/3D-BN	19.28%	1.15	522.73	Mechanic mixing, 3	2020 [52]
ER/3D-BN	10%	0.9	409.09	Salt template, 3	2020 [53]
CNF/3D-BN	27.27%	1.66	401.94	Freeze dry and cross-linking, 5	2021 [54]
PDMS/3D-BN	13.53%	1.58	790.00	Foaming method, 4	2020 [30]
TPU/3D-BN	18.33%	0.48	240.00	Spray drying, 5	2021 [55]
PCL/3D-BN	13.41%	1.01	505.00	Ice template, 4	2020 [56]
PVDF/3D-BN/ER	12.9%	1.2	545.45	NaCl template, 4	2020 [57]
ER/3D-BN	25%	1.13	627.78	Chemical modified, 6	2020 [58]
ER/3D-BN/C	23%	1.52	760.00	NaCl template, 4	2021 [59]
PI/3D-BN/Al_2O_3	12.5%	1.01	561.11	PDA chemistry, 3	2020 [60]
PCC/3D-BN/CNT	9.64%	1.21	239.70	Assembly method, 4	2020 [61]
PDMS/3D-BN/Go	9.16%	1.65	750.00	Hydrothermal, Freeze dry, 5	2020 [62]
ER/3D-BN/Ag	27.08%	0.80	363.64	Ice template, 4	2019 [63]
ER/3D-BN/Ag	25%	2.14	972.73	Chemistry modification, 6	2020 [58]
ER/3D-BN/NF	19.35%	1.19	540.09	Ice template, 4	2021 [64]
PS/3D-BN/Go	5.8%	0.26	173.33	Mechanic mixing, 2	2020 [65]
ER/3D-BP@Ni	6.71%	2.01	908.53	Heat treatment, 1	This work

The fastest heating rates increased with the improvement of thermal conductivity, and the corresponding elapsed time was shorter. After incorporating Ni foam, the final equilibrium temperature of the composite got an enhancement from 58.5 °C to 60.4 °C. The reason was that Ni foam can build smooth phonon pathways inside epoxy. Undoubtedly, the highest final equilibrium temperature of ER/3D-BP@Ni composite was attributed to the continuous and high-quality 3D-BP@Ni network with high thermal conductivity. The temperature distributions on the surface of epoxy and the composites were intuitively observed through the images captured by the infrared thermal imager in the inset of Fig. 6 (a). Evidently, the temperature distribution on the surface of the composites was not as uniform as epoxy. The area of ~25 × 25 was selected on the samples surface to analyze their microscopic temperature distribution at the elapsed time of 180s. In Fig. 6(b) the 3D local temperature distribution of epoxy was low and uniformed. When the 3D skeleton was embedded in epoxy, the heat of temperature resistor was first quickly transferred to the upper surface of the composites through the skeleton. Therefore, the hill-like temperature distribution appeared in Fig. 6(c) and (d). A large area of low temperature region was seen in the local temperature distribution of ER/Ni composite (in Fig. 6(c), view form (90°, −90°)). The phenomenon was caused by the poor interfacial adhesion between Ni foam and epoxy. Although the 3D local temperature distribution of ER/3D-BP@Ni composite was also wave-like (in Fig. 6(d), view from (45°, −45°)), the high heat transferring capacity of 3D-BP@Ni and the strong interfacial adhesion between 3D-BP@Ni and epoxy obviously dispersed low temperature regions and reduced the low temperature area (in Fig. 6(d), view from (90°, −90°)). The phenomenon confirmed that the continuous 3D-BP@Ni network played a critical role in the heat dissipation of the composite. The large area of temperature distributions of epoxy and the composites were shown in Fig. S7. The trend was consistent with the inset of Fig. 6(a). Consequently, the heat generated by electronic devices during operation can be effectively transferred to the heat dissipation system, ensuring the safety of electronic devices, and extending its service life.

3.5. Dimensional and thermal stability of ER composites

For electronic packaging materials, excellent dimensional and thermal stability are necessary [66]. An appropriate CTE value efficiently reduced the thermal stress and microcracks and has been regarded as an important parameter related to reliability in electronic devices. The CTE curves of epoxy and the composites as a function of temperature were shown in Fig. 7(a). The incorporated 3D networks obviously restricted the thermal dimensional deformation of epoxy, especially 3D-BP@Ni network. Compared with pure epoxy, the CTE value of ER/Ni composite was only slightly reduced because of the intrinsic CTE of Ni and poor interface adhesion between Ni and epoxy [67]. The CTE value of ER/3D-BP@Ni composite (26.95×10^{-6}/°C, as shown in Fig. 7(b)) was expectedly lowest and demonstrated an excellent dimensional stability. The main reason was that BP crystal had a low intrinsic CTE value of ~3 $\times 10^{-6}$/°C [35,45]. In detail, the mobility of epoxy molecular chain was constrained in the continuous and high-quality 3D-BP@Ni network due to the strong interface between epoxy and 3D-BP@Ni.

Thermal stabilities of epoxy and the composites, as the other parameter to evaluate the reliability, were investigated by TGA. The TGA curves were presented in Fig. 7(c), from which it was observed that epoxy began to decompose at 280 °C. As for the composites, thermal decomposed temperatures were slightly increased as shown in the inset of Fig. 7(c). Interestingly, the thermal decomposed temperature of ER/3D-BP@Ni composite with high thermal conductivity was lower than that of ER/Ni composite. It indicated that Ni foam promotes the epoxy thermal stability. When BP grains grew on the surface of Ni foam, 3D-BP@Ni endowed with high thermal conductivity was conducive to accelerate the decomposition of epoxy [68]. Nevertheless, the thermal stability of ER/3D-BP@Ni composite was still higher than that of pure epoxy. It can better hinder the diffusion of volatile decomposition

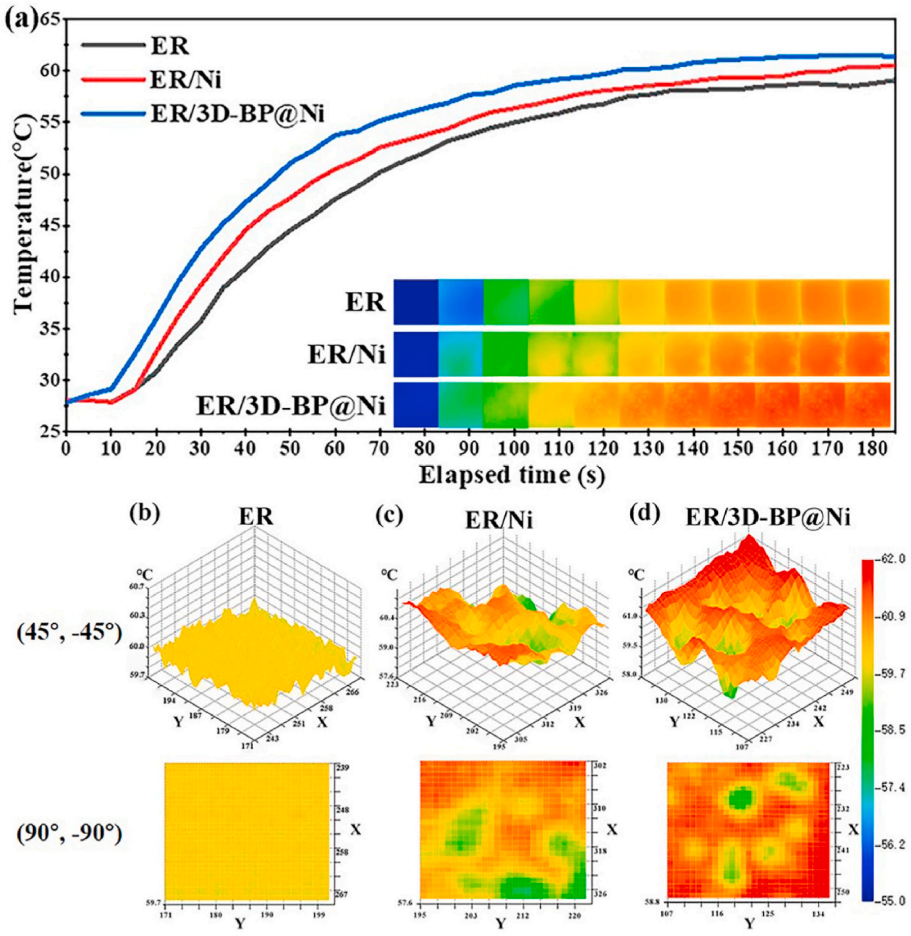

Fig. 6. The heat transfer evolution and the illustration of the infrared thermograph of epoxy and the composites: (a) the surface temperature variations against elapsed time at the heating, infrared thermal images of integrated chip packaging casted with ER composites in the inset, (b) the 3D local temperature distribution of epoxy, (c) the 3D local temperature distribution of ER/Ni composite, (d) the 3D local temperature distribution of ER/3D-BP@Ni composite.

Table 2
The specific elapsed time and rate of the fastest temperature rise and the final equilibrium temperature during the thermal imaging test of epoxy and the composites.

Samples	ER	ER/Ni	ER/3D-BP@Ni
Time/s	30.05	22.27	18.96
Rate/(°C/s)	0.54	0.72	0.74
Temperature/°C	58.5	60.4	63.2

products within the composites. The slight decrease in the thermal decomposition of ER/3D-BP@Ni composite compared with ER/Ni composite does not affect the reliability in working.

To obtain a deeper understanding of the dynamic decomposition process and the thermal stability of epoxy and the composites, kinetic parameters (including polymer decomposition temperature (PDT), integral procedural decomposition temperature (IPDT)) based on Doyle's proposition were determined from the TGA curves and calculated, according to the equations in Supplementary, S6. All results were presented in Table 3. IPDT was usually used to characterize the volatile part of polymer and to assess the inherent thermal stability [69]. IPDT values of the composites exceeded that of pure epoxy, indicating the thermal stability increased. The Horowitz–Metzger method was used to calculate the activation energy of epoxy and the composites, according to equation (1):

$$\ln\left(\ln(1-\alpha)^{-1}\right) = \frac{E}{RT_{max}^2}\theta \quad (1)$$

where E was the activation energy for decomposition process, α was the decomposed fraction, T_{max} was the temperature at the maximum weight loss rate, θ was the variable auxiliary temperature defined as $\theta = T - T_{max}$, and R was the real gas constant (8.314 J/(mol·K)) [70]. The plots of ln[ln(1-α)-1] versus θ were shown in Fig. 7(d). The activation energy (E, in Table 2) was calculated by fitting the slope in Fig. 7(d). Generally, the larger the value of E, the higher energy was required for the composites to be decomposed, and the stronger the thermal stability. The composites had higher E values than pure epoxy resin, indicating that networks were beneficial to improve the thermal stability. Consistent with expectation, ER/3D-BP@Ni composite not only had the highest IPDT, but also had the largest E value.

4. Conclusions

Three-dimensional boron phosphide@nickel (3D-BP@Ni) structure was designed and fabricated using a 3D template of commercial Ni foam by one-step high temperature treatment. The results showed the Ni foam was completely covered by high-quality BP grains. Although the layer thickness of BP grains was only a few microns, 3D-BP@Ni was endowed with a faster thermal response than that of Ni foam and traditional 3D BN networks. In comparison with the polymer composites containing 3D BN networks, the thermal conductivity of ER/3D-BP@Ni composite represented a great improvement. In addition, the incorporation of 3D-

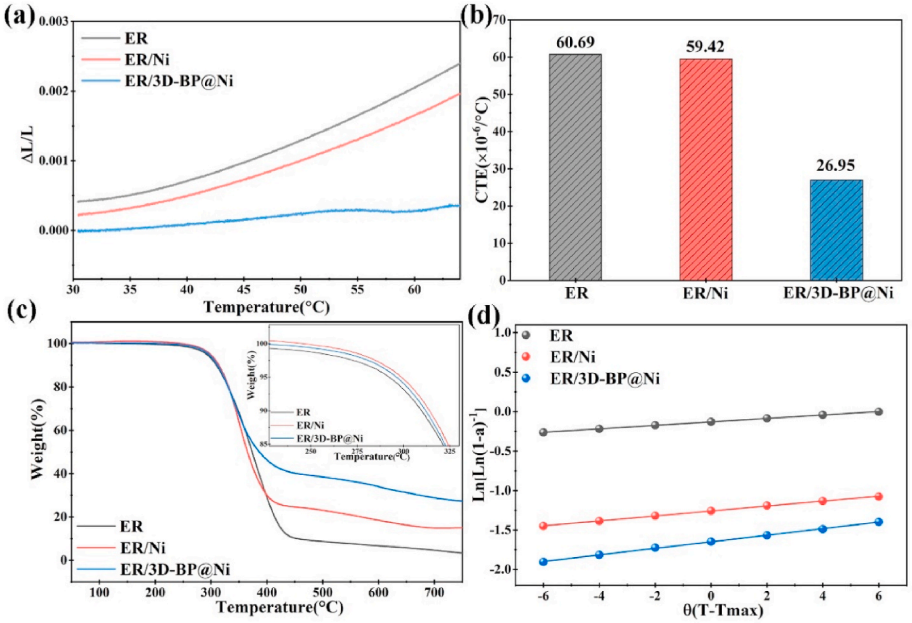

Fig. 7. Dimensional and thermal stability of epoxy and the composites: (a) the CTE curve, (b) the CTE value, (c) the thermal decomposition curve, (d) the plots of ln [ln(1 − α)−1] versus θ using Horowitz-Metzger method.

Table 3
Thermal stabilities of the composites obtained from TGA curves.

Samples	Td5 (°C)	Td50 (°C)	Tmax (°C)	PDT (°C)	IPDT (°C)	*E*(kJ/mol)
ER	292.2	374.6	384.0	282.2	412.0	268.6
ER/Ni	299.0	365.2	328.0	297.2	599.6	280.1
ER/3D-BP@Ni	296.3	386.6	338.0	291.9	870.1	394.9

BP@Ni also reduced the coefficient of thermal expansion (CTE). The improved performances of the composites were attributed to high-quality and good integrity of continuous 3D-BP@Ni network and the strong interfaces between epoxy and 3D-BP@Ni network. The developed 3D-BP@Ni network combining the high thermal conductivity of BP and the inherent advantages of the 3D network offers a new design strategy for high-efficiency thermal management materials.

Credit authorship contribution statement

Jing He: Conceptualization, Data curation, Writing-original draft. Hua Wang: Experiments Supervision, Data Curation.Yi Gong: Investigation.Xingyou Tian: Project administration, Supervision.Zhiliang Zhang: Writing-review&editing.Jianying He: Validation, Writing-review&editing, Project administration.

Declaration of competing interest

The authors declare that they have no known competing financial interests or personal relationships that could have appeared to influence the work reported in this paper.

Acknowledgments

The authors would like to acknowledge the financial support from National Key R&D Program of China (No. 2017YFB0406200); the Research Council of Norway (No. 251068, Engineering Metal–Polymer Interface for Enhanced Heat Transfer; and No. 295864, the Norwegian Micro- and Nano-Fabrication Facility); Supported by the CASHIPS Director's Fund (No. YZJJZX202015); "Strategic Priority Research Program" of the Chinese Academy of Science (No. XDA13040505); Science and Technology Service Network Initiative of the Chinese Academy of Sciences (guide project for innovative and entrepreneurial, KFJ-STS-SCYD-112); Key deployment project of the Chinese Academy of Sciences (KFZD-SW-416); and Science and Technology Cooperation Project of Sichuan Province and the Chinese Academy of Sciences (2017JZ0028).

Appendix A. Supplementary data

Supplementary data to this article can be found online at https://doi.org/10.1016/j.compositesb.2022.109662.

References

[1] Ball P. Computer engineering: feeling the heat. Nature 2012;492(7428):174–6.
[2] Wu Y, Ordonez-Miranda J, Gluchko S, Anufriev R, Meneses DDS, Del Campo L, et al. Enhanced thermal conduction by surface phonon-polaritons. Sci Adv 2020;6(40):eabb4461.
[3] Waldrop MM. The chips are down for Moore's law. Nature 2016;530(7589):144–7.
[4] van Erp R, Soleimanzadeh R, Nela L, Kampitsis G, Matioli E. Co-designing electronics with microfluidics for more sustainable cooling. Nature 2020;585(7824):211–6.
[5] Kim D, Yamamoto Y, Nagao S, Wakasugi N, Chen C, Suganuma K. Measurement of heat dissipation and thermal-stability of power modules on DBC substrates with various ceramics by SiC micro-heater chip system and Ag sinter joining. Micromachines 2019;10(11).
[6] Li J, Zhang X, Zhou C, Zheng J, Ge D, Zhu W. New applications of an automated system for high-power LEDs. IEEE/ASME Transactions on Mechatronics. 2016;21(2):1035–42.
[7] Li S, Zheng Q, Lv Y, Liu X, Wang X, Huang PY, et al. High thermal conductivity in cubic boron arsenide crystals. Science 2018;361(6402):579–81.
[8] Huang C, Qian X, Yang R. Thermal conductivity of polymers and polymer nanocomposites. Mater Sci Eng R Rep 2018;132:1–22.
[9] He J, Wang H, Qu Q, Su Z, Qin T, Da Y, et al. Self-assembled three-dimensional structure with optimal ratio of GO and SiC particles effectively improving the thermal conductivity and reliability of epoxy composites. Composites Communications 2020;22:100448.
[10] Shen X, Zheng Q, Kim J-K. Rational design of two-dimensional nanofillers for polymer nanocomposites toward multifunctional applications. Prog Mater Sci 2020:100708.
[11] Xu Y, Kraemer D, Song B, Jiang Z, Zhou J, Loomis J, et al. Nanostructured polymer films with metal-like thermal conductivity. Nat Commun 2019;10(1):1771.
[12] Zhai S, Zhang P, Xian Y, Zeng J, Shi B. Effective thermal conductivity of polymer composites: theoretical models and simulation models. Int J Heat Mass Tran 2018;117:358–74.

[13] Li J, Li X, Zheng Y, Liu Z, Tian Q, Liu X. New underfill material based on copper nanoparticles coated with silica for high thermally conductive and electrically insulating epoxy composites. J Mater Sci 2019;54(8):6258–71.
[14] Yao Y, Zeng X, Wang F, Sun R, Xu J-b, Wong C-P. Significant enhancement of thermal conductivity in bioinspired freestanding boron nitride papers filled with graphene oxide. Chem Mater 2016;28(4):1049–57.
[15] Xiao C, Guo Y, Tang Y, Ding J, Zhang X, Zheng K, et al. Epoxy composite with significantly improved thermal conductivity by constructing a vertically aligned three-dimensional network of silicon carbide nanowires/boron nitride nanosheets. Compos B Eng 2020;187:107855.
[16] Lian G, Tuan C-C, Li L, Jiao S, Wang Q, Moon K-S, et al. Vertically aligned and interconnected graphene networks for high thermal conductivity of epoxy composites with ultralow loading. Chem Mater 2016;28(17):6096–104.
[17] Chen H, Ginzburg VV, Yang J, Yang Y, Liu W, Huang Y, et al. Thermal conductivity of polymer-based composites: fundamentals and applications. Prog Polym Sci 2016;59:41–85.
[18] Cui Y, Bao D, Xu F, Gao Y, Zhang X, Geng H, et al. Fabrication of EVA connected 3D BN network for enhancing the thermal conductivity of epoxy composites. Compos B Eng 2021;224:109203.
[19] Xu T, Zhou S, Jiang F, Song N, Shi L, Ding P. Polyamide composites with improved thermal conductivity for effective thermal management: the three-dimensional vertically aligned carbon network. Compos B Eng 2021;224:109205.
[20] Anufriev R, Nomura M. Ray phononics: thermal guides, emitters, filters, and shields powered by ballistic phonon transport. Materials Today Physics 2020;15:100272.
[21] Fu B, Ren P, Guo Z, Du Y, Jin Y, Sun Z, et al. Construction of three-dimensional interconnected graphene nanosheet network in thermoplastic polyurethane with highly efficient electromagnetic interference shielding. Compos B Eng 2021;215:108813.
[22] Gong X, Sang Z, Guo H, Ke K, Manas-Zloczower I, Feke DL. Piezoresistive strain sensors based on psyllium-carbon nanostructure skeletons. Compos B Eng 2021;209:108610.
[23] Zakaria MR, Md Akil H, Abdul Kudus MH, Ullah F, Javed F, Nosbi N. Hybrid carbon fiber-carbon nanotubes reinforced polymer composites: a review. Compos B Eng 2019;176:107313.
[24] Lai KC, Lee LY, Hiew BYZ, Thangalazhy-Gopakumar S, Gan S. Environmental application of three-dimensional graphene materials as adsorbents for dyes and heavy metals: review on ice-templating method and adsorption mechanisms. Journal of Environmental Sciences 2019;79:174–99.
[25] Chen W, Li S, Chen C, Yan L. Self-assembly and embedding of nanoparticles by in situ reduced graphene for preparation of a 3D graphene/nanoparticle aerogel. Adv Mater 2011;23(47):5679–83.
[26] Zeng J, Ji X, Ma Y, Zhang Z, Wang S, Ren Z, et al. 3D graphene fibers grown by thermal chemical vapor deposition. Adv Mater 2018;30(12):1705380.
[27] Li Y, Tian X, Yang W, Li Q, Hou L, Zhu Z, et al. Dielectric composite reinforced by in-situ growth of carbon nanotubes on boron nitride nanosheets with high thermal conductivity and mechanical strength. Chem Eng J 2019;358:718–24.
[28] Zeng X, Yao Y, Gong Z, Wang F, Sun R, Xu J, et al. Ice-templated assembly strategy to construct 3D boron nitride nanosheet networks in polymer composites for thermal conductivity improvement. Small 2015;11(46):6205–13.
[29] Tian X, Pan T, Deng B, Zhang H, Li Y, Li Q, et al. Synthesis of sandwich-like nanostructure fillers and their use in different types of thermal composites. ACS Appl Mater Interfaces 2019;11(43):40694–703.
[30] Liu Z, Li J, Liu X. Novel functionalized BN nanosheets/epoxy composites with advanced thermal conductivity and mechanical properties. ACS Appl Mater Interfaces 2020;12(5):6503–15.
[31] Tian X, Wu N, Zhang B, Wang Y, Geng Z, Li Y. Glycine functionalized boron nitride nanosheets with improved dispersibility and enhanced interaction with matrix for thermal composites. Chem Eng J 2021;408:127360.
[32] Xiao C, Tang Y, Chen L, Zhang X, Zheng K, Tian X. Preparation of highly thermally conductive epoxy resin composites via hollow boron nitride microbeads with segregated structure. Compos Appl Sci Manuf 2019;121:330–40.
[33] Su Z, Wang H, Tian K, Huang W, Xiao C, Guo Y, et al. The combination of π-π interaction and covalent bonding can synergistically strengthen the flexible electrical insulating nanocomposites with well adhesive properties and thermal conductivity. Compos Sci Technol 2018;155:1–10.
[34] Slack GA. Nonmetallic crystals with high thermal conductivity. J Phys Chem Solid 1973;34(2):321–35.
[35] Tian F, Ren Z. High thermal conductivity in boron arsenide: from prediction to reality. Angew Chem Int Ed 2019;58(18):5824–31.
[36] Popper P, Ingles T. Boron phosphide, a III–V compound of zinc-blende structure. Nature 1957;179(4569):1075.
[37] Kang JS, Wu H, Hu Y. Thermal properties and phonon spectral characterization of synthetic boron phosphide for high thermal conductivity applications. Nano Lett 2017;17(12):7507–14.
[38] Zheng Q, Li S, Li C, Lv Y, Liu X, Huang PY, et al. High thermal conductivity in isotopically enriched cubic boron phosphide. Adv Funct Mater 2018;28(43):1805116.
[39] Shin S, Wang Q, Luo J, Chen R. Advanced materials for high-temperature thermal transport. Adv Funct Mater 2019;30(8):1904815.
[40] Lindsay L, Broido DA, Reinecke TL. First-principles determination of ultrahigh thermal conductivity of boron arsenide: a competitor for diamond? Phys Rev Lett 2013;111(2):025901.
[41] Kumashiro Y, Mitsuhashi T, Okaya S, Muta F, Koshiro T, Takahashi Y, et al. Thermal conductivity of a boron phosphide single-crystal wafer up to high temperature. J Appl Phys 1989;65(5):2147–8.
[42] Stone B, Hill D. Semiconducting properties of cubic boron phosphide. Phys Rev Lett 1960;4(6):282–4.
[43] Woo K, Lee K, Kovnir K. BP: synthesis and properties of boron phosphide. Mater Res Express 2016;3(7):074003.
[44] Solozhenko VL, Bushlya V. Mechanical properties of boron phosphides. J Superhard Mater 2019;41(2):84–9.
[45] Li S, Taddei KM, Wang X, Wu H, Neuefeind J, Zackaria D, et al. Thermal expansion coefficients of high thermal conducting BAs and BP materials. Appl Phys Lett 2019;115(1):011901.
[46] Jia ZC, Zhu JQ, Jiang CZ, Shen WX, Han JC, Chen RR. Effect of gas flow ratio on the microstructure and mechanical properties of boron phosphide films prepared by reactive magnetron sputtering. Appl Surf Sci 2011;258(1):356–60.
[47] Padavala B, Frye CD, Ding Z, Chen R, Dudley M, Raghothamachar B, et al. Preparation, properties, and characterization of boron phosphide films on 4H- and 6H-silicon carbide. Solid State Sci 2015;47:55–60.
[48] Sugimoto H, Somogyi B, Nakamura T, Zhou H, Ichihashi Y, Nishiyama S, et al. Size-dependent photocatalytic activity of cubic boron phosphide nanocrystals in the quantum confinement regime. J Phys Chem C 2019;123(37):23226–35.
[49] Mou S, Wu T, Xie J, Zhang Y, Ji L, Huang H, et al. Boron phosphide nanoparticles: a nonmetal catalyst for high-selectivity electrochemical reduction of CO2 to CH3OH. Adv Mater 2019;31(36):1903499.
[50] Chu TL, Jackson JM, Smeltzer RK. The crystal growth of boron monophosphide from metal phosphide solutions. J Electrochem Soc 1973;120(6):802.
[51] Yao Q, Qu J. Interfacial versus cohesive failure on polymer-metal interfaces in electronic packaging—effects of interface roughness. J Electron Packag 2002;124(2):127–34.
[52] Zhao L, Yan L, Wei C, Li Q, Huang X, Wang Z, et al. Synergistic enhanced thermal conductivity of epoxy composites with boron nitride nanosheets and microspheres. J Phys Chem C 2020;124(23):12723–33.
[53] Xu X, Hu R, Chen M, Dong J, Xiao B, Wang Q, et al. 3D boron nitride foam filled epoxy composites with significantly enhanced thermal conductivity by a facial and scalable approach. Chem Eng J 2020;397:125447.
[54] Wang X, Qu Y, Jiao L, Bian H, Wang R, Wu W, et al. Boosting the thermal conductivity of CNF-based composites by cross-linked lignin nanoparticle and BN-OH: dual construction of 3D thermally conductive pathways. Compos Sci Technol 2021;204:108641.
[55] Su K-H, Su C-Y, Chi P-W, Chandan P, Cho C-T, Chi W-Y, et al. Generation of self-assembled 3D network in TPU by insertion of Al2O3/h-BN hybrid for thermal conductivity enhancement. Materials 2021;14(2):238.
[56] Wu F, Chen S, Tang X, Fang H, Tian H, Li D, et al. Thermal conductivity of polycaprolactone/three-dimensional hexagonal boron nitride composites and multi-orientation model investigation. Compos Sci Technol 2020;197:108245.
[57] Chen X, Lim JSK, Yan W, Guo F, Liang YN, Chen H, et al. Salt template Assisted BN scaffold fabrication toward highly thermally conductive epoxy composites. ACS Appl Mater Interfaces 2020;12(14):16987–96.
[58] Wu Y, Zhang X, Negi A, He J, Hu G, Tian S, et al. Synergistic effects of boron nitride (BN) nanosheets and silver (Ag) nanoparticles on thermal conductivity and electrical properties of epoxy nanocomposites. Polymers 2020;12(2):426.
[59] Pan D, Li Q, Zhang W, Dong J, Su F, Murugadoss V, et al. Highly thermal conductive epoxy nanocomposites filled with 3D BN/C spatial network prepared by salt template assisted method. Compos B Eng 2021;209:108609.
[60] Duan G, Cao Y, Quan J, Hu Z, Wang Y, Yu J, et al. Bioinspired construction of BN@polydopamine@Al2O3 fillers for preparation of a polyimide dielectric composite with enhanced thermal conductivity and breakdown strength. J Mater Sci 2020;55(19):8170–84.
[61] Xia Y, Li Q, Ji R, Zhang H, Xu F, Huang P, et al. Multielement synergetic effect of boron nitride and multiwalled carbon nanotubes for the fabrication of novel shape-stabilized phase-change composites with enhanced thermal conductivity. ACS Appl Mater Interfaces 2020;12(37):41398–409.
[62] Liu C, Wu W, Wang Y, Liu X, Chen Q, Xia S. Silver nanoparticle-enhanced three-dimensional boron nitride/reduced graphene oxide skeletons for improving thermal conductivity of polymer composites. ACS Applied Polymer Materials 2021;3(7):3334–43.
[63] Fu C, Yan C, Ren L, Zeng X, Du G, Sun R, et al. Improving thermal conductivity through welding boron nitride nanosheets onto silver nanowires via silver nanoparticles. Compos Sci Technol 2019;177:118–26.
[64] Yao T, Chen K, Niu T, Yang Y. Effects of frequency and thermal conductivity on dielectric breakdown characteristics of epoxy/cellulose/BN composites fabricated by ice-templated method. Compos Sci Technol 2021;213:108945.
[65] Jiang F, Cui X, Song N, Shi L, Ding P. Synergistic effect of functionalized graphene/boron nitride on the thermal conductivity of polystyrene composites. Composites Communications 2020;20:100350.
[66] Ma J, Shang T, Ren L, Yao Y, Zhang T, Xie J, et al. Through-plane assembly of carbon fibers into 3D skeleton achieving enhanced thermal conductivity of a thermal interface material. Chem Eng J 2020;380:122550.
[67] Kollie TG. Measurement of the thermal-expansion coefficient of nickel from 300 to 1000 K and determination of the power-law constants near the Curie temperature. Phys Rev B 1977;16(11):4872–81.

[68] Wu Z, Xue M, Wang H, Tian X, Ding X, Zheng K, et al. Electrical and flame-retardant properties of carbon nanotube/poly(ethylene terephthalate) composites containing bisphenol A bis(diphenyl phosphate). Polymer 2013;54(13):3334–40.
[69] He J, Wang H, Qu Q, Su Z, Qin T, Tian X. Three-dimensional network constructed by vertically oriented multilayer graphene and SiC nanowires for improving thermal conductivity and operating safety of epoxy composites with ultralow loading. Compos Appl Sci Manuf 2020;139:106062.
[70] Su Z, Wang H, He J, Guo Y, Qu Q, Tian X. Fabrication of thermal conductivity enhanced polymer composites by constructing an oriented three-dimensional staggered interconnected network of boron nitride platelets and carbon nanotubes. ACS Appl Mater Interfaces 2018;10(42):36342–51.